

Multiplicity of Steady State Solutions in 2-D Incompressible Viscous Wall Driven Arc-Shaped Cavity Flow

E. Erturk[†]

Bahcesehir University, School of Applied Disciplines, Istanbul, Turkey

[†]Corresponding Author Email: ercan.erturk@eng.bau.edu.tr

(Received October 6, 2020; accepted December 29, 2020)

ABSTRACT

Numerical simulations of the steady 2-D incompressible viscous flow in an arc-shaped cavity are presented. The Navier–Stokes equations in streamfunction and vorticity formulation are solved numerically using a body fitted mesh obtained by a conformal mapping. Our numerical results reveal that the arc-shaped cavity flow has multiple steady solutions above a bifurcation Reynolds number when the arc length ratio is less than 1/2 ($r < 1/2$). Multiple steady state solutions of the arc-shaped cavity flow with different arc length ratios ($r = 2/5, 1/3, 1/4, 1/5$ and $1/6$) are presented at a variety of Reynolds numbers. Our results show that the bifurcation Reynolds number at which a second solution starts to exist changes as the arc length ratio of the arc-shaped cavity changes. Among the considered different arc length ratios ($r = 2/5, 1/3, 1/4, 1/5$ and $1/6$), the minimum bifurcation Reynolds number occurs at 1/3 arc length ratio with $Re = 5164$. Detailed results are presented.

Keywords: Arc-shaped cavity flow; Multiple steady state solutions; Bifurcation Reynolds number; 2-D incompressible viscous flow; Arc length ratio.

1. INTRODUCTION

The Navier-Stokes equations which govern the flow of a viscous fluid constitute a nonlinear system of equations. The governing nonlinear flow equations can exhibit multiple steady solutions for some particular flow problems, see (Shankar and Deshpande (2000)). Multiple solutions of any particular flow problem is both fascinating and interesting to fluid dynamics researchers. In the literature it is possible to find studies that present multiple steady numerical solutions of some particular flow problems having the same boundary conditions at the same Reynolds number. Two-sided (two facing side) driven rectangular cavity flow and also two- (two non-facing side) and four-sided driven square cavity flow are examples of flow problems that have multiple steady solutions above a bifurcation Reynolds number from the literature.

Albensoeder *et al.* (2001) have studied the twodimensional steady incompressible flow in a rectangular cavity using a finite volume method which is driven by two facing side walls. They (Albensoeder *et al.* (2001)) found several bifurcations in the solution of the flow and presented different non-unique two-dimensional steady solutions of the rectangular flow with different aspect ratios at different Reynolds numbers. Similar

to Albensoeder *et al.* (2001), Chen *et al.* (2013) have also presented multiple steady solutions of the two-sided (facing walls) driven flow in a rectangular cavity with different aspect ratios.

In the literature, multiple steady solutions of flow in a square cavity are presented by Lemée *et al.* (2015) and Prasad and Dass (2016) which is driven by two opposite facing walls, by Wahba (2009) and Perumal and Dass (2011) which is driven by two non-facing and also driven by four side walls respectively, by Zhuo *et al.* (2015) which is driven by four side walls.

The flow problems in enclosures mentioned above, ie. rectangular or square cavity flows driven by two facing side walls or two non-facing opposite side walls or four side walls, that have multiple steady solutions presented in Albensoeder *et al.* (2001), Chen *et al.* (2013), Lemée *et al.* (2015), Prasad and Dass (2016), Wahba (2009), Perumal and Dass (2011), Zhuo *et al.* (2015) have two different type of solutions, mirror symmetric and non-symmetric. These flow problems actually have a mirror symmetry line due to the mirror symmetry in geometry and also due to the mirror symmetry in the boundary conditions.

Flows in different enclosures always attract the Computational Fluid Dynamics (CFD) community since these flows usually have simple geometries

which are easy to apply CFD techniques in terms of coding while on the other hand they retain complex flow physics in just a simple geometry. Glowinski *et al.* (2006) introduced the driven semicircular cavity flow problem. They (Glowinski *et al.* 2006) solved the governing flow equations using unsteady operator-splitting/finite elements method on an unstructured mesh. Later Yang *et al.* (2012), Ding *et al.* (2009), have also studied the semi-circular cavity flow problem numerically. Migeon *et al.* (2000) conducted experiments and studied the flow establishment inside semi-circular cavity together with square and rectangular cavities.

In the literature, Mercan and Atalik (2009) also studied the semi-circular cavity flow problem. Apart from Glowinski *et al.* (2006), Yang *et al.* (2012), and Ding *et al.* (2009) in their study Mercan and Atalik (2009) also introduced arc-shaped cavity flow with different arc length ratios which is a variety of the semi-circular cavity flow. They (Mercan and Atalik (2009)) have presented high Reynolds number solutions arc-shaped cavity flow with different arc length ratios.

In Mercan and Atalik (2009), only at the arc-shaped cavity flow with arc length ratios less than 1/2 (ie. 1/3, 1/4 and 1/5) we realize that at high Reynolds the flow topology changes dramatically. While investigating these dramatic changes in the flow topology, we reveal that the arc-shaped cavity flow with arc length ratios less than 1/2 have multiple steady solutions (at least two different solutions so far with this study) above a bifurcation Reynolds number. In their study, most probably without noticing the multiplicity in the steady solution Mercan and Atalik (2009) have presented different multiple solutions of the arc-shaped cavity flow as the behavior of the unique solution with increasing the Reynolds number.

The arc-shaped cavity flow problem do not have a mirror symmetry line and therefore do not have a symmetric solution. To the best of our knowledge, in the literature there is not any example of flows in enclosures with a driven wall that has multiple steady solutions with non of them being symmetric. In this sense most probably the arc-shaped driven cavity flow is a unique flow example that has multiple non-symmetric steady solutions in the literature to the best of our knowledge. In this study, we present multiple steady solutions of arc-shaped cavity flow with various arc length ratios which are all less than 1/2 at various Reynolds numbers. In order to obtain a body fitted mesh, we use complex algebra that conformally maps the considered semicircular geometry into an infinite half domain analytically. The streamfunction and vorticity equations are solved iteratively for the wall-driven arcshaped cavity flow. By varying the Reynolds number we obtain the bifurcation Reynolds numbers of the arc-shaped cavity flow which the solution change behavior and start to have multiple solutions. Detailed results are presented.

cavity flow problem and considered arcshaped cavity with different arc length ratios

2. NUMERICAL METHOD

The flow problem at hand, the arc-shaped cavity flow, has a geometry that has the portion of a circle as shown in Fig. 1a. We follow Mercan and Atalik (2009) and characterize the arc-shaped cavity by the ratio (r) of the arc length of the curved bottom surface to the full angle which is equal to 2π . The $r=1/2$ case which is the semi circle cavity was studied extensively in Glowinski *et al.* (2006), Yang *et al.* (2012), Ding *et al.* (2009), Mercan and Atalik (2009). In this study we will only concentrate on the arc-shaped cavity geometries with arc length ratio less than 1/2 in which the flow has multiple steady state solutions. Following Mercan and Atalik (2009) in this study we consider arc-shaped cavities with 1/3, 1/4 and 1/5 ratios which are are less than 1/2. Additional to these ratios, in these study we also consider the arc-shaped cavity with $r=2/5$ and $r=1/6$. As seen in Fig. 1a the top lid of the arc-shaped cavity is a chord line of a circle. For all the ratios (r) considered in this study the width of the top lid, ie. the chord, is equal to unity ($L=1$). Also as shown in Fig. 1a, the top lid moves with a velocity that is equal to unity ($U=1$). The arc-shaped cavity with different arc length ratios considered in this study are given in Fig. 1b all together for easy comparison.

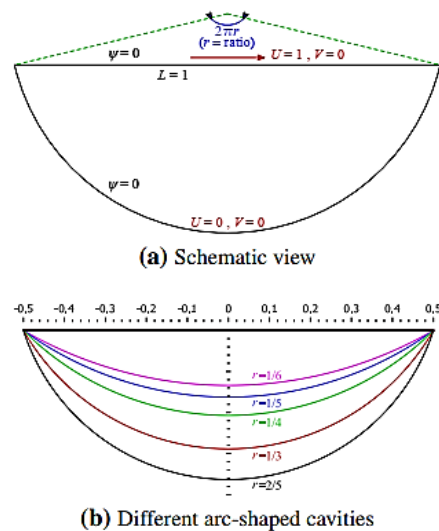


Fig. 1. Schematic view of the wall-driven arcshaped.

The steady incompressible two-dimensional viscous flow inside the arc-shaped cavity is governed by the Navier-Stokes equation and we use the streamfunction and vorticity formulation of the N-S equations, such that

$$\psi_{xx} + \psi_{yy} = \omega \tag{1}$$

$$\psi_y \omega_x - \psi_x \omega_y = \frac{1}{Re} (\omega_{xx} + \omega_{yy}) \tag{2}$$

where the Reynolds number (Re) is based on the top lid velocity (U) and the width of the top lid (L).

2.1 Governing Equations in Curvilinear Coordinates

For the solution of the flow problem, we map the physical domain into a rectangular computational domain. The governing streamfunction Eq. (1) and vorticity Eq. (2) in curvilinear coordinates are given as

$$\frac{\alpha\psi_{\xi\xi} - 2\beta\psi_{\xi\eta} + \gamma\omega_{\eta\eta} + \sigma\psi_{\eta} + \tau\psi_{\xi}}{J^2} = \omega \quad (3)$$

$$\psi_{\eta} \omega_{\xi} - \psi_{\xi} \omega_{\eta} = \frac{1}{Re} \frac{\alpha\omega_{\xi\xi} - 2\beta\omega_{\xi\eta} + \gamma\omega_{\eta\eta} + \sigma\omega_{\eta} + \tau\omega_{\xi}}{J} \quad (4)$$

where the Jacobian of the transformation is given as

$$J = x_{\xi}y_{\eta} - x_{\eta}y_{\xi} \quad (5)$$

and the coordinate system parameters appear as coefficients in the above equations are given as

$$\begin{aligned} \alpha &= x_{\eta}^2 + y_{\eta}^2 \\ \beta &= x_{\xi}x_{\eta} + y_{\xi}y_{\eta} \\ \gamma &= x_{\xi}^2 + y_{\xi}^2 \\ \sigma &= \frac{y_{\xi}(Dx) - x_{\xi}(Dy)}{J} \\ \tau &= \frac{x_{\eta}(Dy) - y_{\eta}(Dx)}{J} \end{aligned} \quad (6)$$

also where Dx and Dy are defined as the following

$$\begin{aligned} Dx &= \alpha x_{\xi\xi} - 2\beta x_{\xi\eta} + \gamma x_{\eta\eta} \\ Dy &= \alpha y_{\xi\xi} - 2\beta y_{\xi\eta} + \gamma y_{\eta\eta} \end{aligned} \quad (7)$$

In this study, only the steady state solutions are of interest. For this reason, as discussed in [Lomax and Steger \(1975\)](#), we use a steady iterative numerical approach in solving the steady governing flow equations. Thus we use the Successive Over Relaxation (SOR) method for the numerical solution of the governing steady streamfunction Eq. (3) and vorticity Eq. (4).

2.2 Body Fitted Mesh

For numerical solution of a partial differential system, a body fitted orthogonal mesh is always desired in computational fluid dynamics. In order to generate the body fitted mesh for the arc-shaped cavity geometry we use the potential flow analysis and consider the superposition of a source and a sink with equal strengths of 2π located at $(-\frac{1}{2}, 0)$ and

$(\frac{1}{2}, 0)$ $x - y$ -coordinates respectively, as shown in

Fig. 2. The arc-shaped cavity geometry can be conformally mapped into a body fitted orthogonal coordinate system using the following complex function

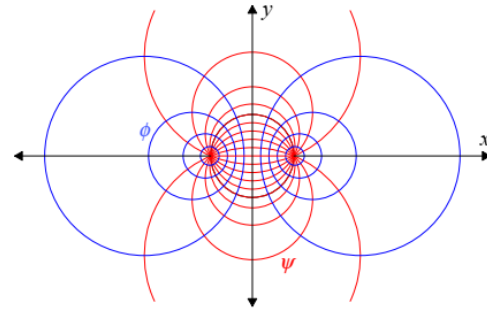


Fig. 2. Constant velocity potential function (blue) and stream function (red) lines of the superposition of the potential flow of a source and sink with equal strengths.

$$w = \log \frac{z - \frac{1}{2}}{z + \frac{1}{2}} \quad (8)$$

Here z is defined as $z = x + iy$ and w is defined as $w = \phi + i\psi$ where ϕ is the velocity potential function and ψ is the stream function.

When we separate the real and imaginary parts of the complex function w in Eq. (8), the real part gives the velocity potential function as

$$\phi = \log \frac{\left| z - \frac{1}{2} \right|}{\left| z + \frac{1}{2} \right|} = \log \frac{\sqrt{\left(z - \frac{1}{2} \right)^2 + y^2}}{\sqrt{\left(z + \frac{1}{2} \right)^2 + y^2}} \quad (9)$$

And similarly the imaginary part gives the stream function as

$$\psi = \arctan \frac{y}{x - \frac{1}{2}} - \arctan \frac{y}{x + \frac{1}{2}} \quad (10)$$

For any constant velocity potential function value (ie. $\phi = c$) rearranging Eq. (9) we obtain

$$x^2 + y^2 + \frac{e^{2c} + 1}{e^{2c} - 1} x + \frac{1}{4} = 0 \quad (11)$$

This equation represents coaxial circles whose centers are on the x -axis with center coordinates

$$x = -\frac{1}{2} \frac{e^{2c} + 1}{e^{2c} - 1}, y = 0$$

and also with radii that are equal to $r = \frac{1}{2} \sqrt{\left(\frac{e^{2c} + 1}{e^{2c} - 1} \right)^2 - 1}$. These coaxial

circles are shown with blue color in Fig. 2.

Following the same procedure, for any constant stream function value (ie. $\psi = c$) rearranging Eq. (10) we obtain

$$x^2 + y^2 - \frac{y}{\tan c} - \frac{1}{4} = 0 \quad (12)$$

This equation represents coaxial circles whose centers are on the y-axis. These coaxial circles are shown with red color in Fig. 2. The center coordinates of these circles are $x = 0, y = \frac{1}{2} \tan c$. Also these circles have radii that are equal to $r = \frac{1}{2} \sqrt{\frac{1}{(\tan c)^2} + 1}$. All of these circles with different radii pass through the source and the sink locations, i.e. through the points $(-\frac{1}{2}, 0)$ and $(\frac{1}{2}, 0)$. We note that the straight line connecting the $(-\frac{1}{2}, 0)$ and $(\frac{1}{2}, 0)$ points constitutes the top lid of the arc-shaped cavity. Also the bottom curved surface of the arc-shaped cavity coincides with the appropriate $\psi = c$ line depending on the considered arc length ratio.

Using equations 11 and 12 we obtain the grid points inside the arc-shaped cavity. We choose the number of grid points such that the aspect ratio of the grid spacing $\left(\frac{\Delta x}{\Delta y}\right)$ is around unity in most of the computational domain, for example for $r=2/5$ arc-shaped cavity we used 600×110 grid points in the mesh. At the top lid of the arc-shaped cavity we used 600 equally spaced grid points and we obtain the velocity potential function values ($\phi = c$) at these grid points. Similarly at the vertical line in the mid of the arc-shaped cavity at $x = 0$ we used 110 equally spaced grid points and we obtain the stream function values ($\psi = c$) at these grid points. In the interior domain the grid points are obtained at the intersection points of these calculated velocity potential lines and the streamfunction lines. Figure 3 shows the mesh we used in this study for considered different arc length ratios (r).

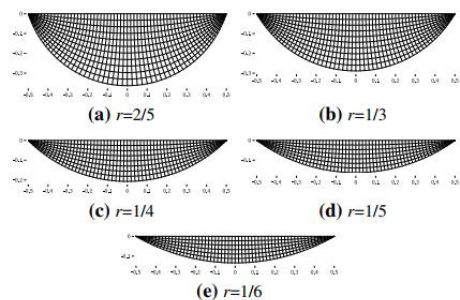


Fig. 3. Body fitted mesh used for arc-shaped cavity (1 out of every 10 grids is shown).

2.3 Transformation Metrics and Wall Boundary Conditions

In order to solve the streamfunction Eq. (3) and vorticity Eq. (4) numerically we need the values of

the mapping transformation metrics that appear in Eqs. (5), (6) and (7). These transformation metrics are calculated numerically using finite difference. For this we transform the body fitted curvilinear mesh in physical space (x,y) to a rectangular uniform mesh in computational space (ξ,η) with uniform grid spacing which is equal to unity ($\Delta\xi=\Delta\eta=1$). Since the transformation metrics appear explicitly in the coefficients of the governing streamfunction Eq. (3) and vorticity Eq. (4), the numerical errors associated with finite difference approximation of the mapping transformation metrics can affect the numerical solution accuracy. For the numerical solution of the streamfunction Eq. (3) and vorticity Eq. (4) we use 3 point second order accurate central differencing, $O(\Delta\xi^2, \Delta\eta^2)$. In finite difference calculation of the transformation metrics we decided to use higher order accuracy and we used fourth order accurate finite differencing, $O(\Delta\xi^4, \Delta\eta^4)$. For the transformation metrics at the interior grid points we use the following 5 point fourth order finite difference equation

$$(f_\eta)_{i,j} = \frac{f_{i,j-2} - 8f_{i,j-1} + 8f_{i,j+1} - f_{i,j+2}}{12} \quad (13)$$

where the subscripts i and j are the grid index and f can be x or y in our case. Using Eq. (13) f_ξ is also calculated similarly. The transformation metrics at the first grid points adjacent to the wall are calculated as the following

$$(f_\eta)_{i,1} = \frac{-3f_{i,0} - 10f_{i,1} + 18f_{i,2} - 6f_{i,3} + f_{i,4}}{12} \quad (14)$$

where the subscripts 0 denotes the grid points on the wall boundary, 1 denotes the first set of grid points adjacent to the wall points and so on. Also at the grid points on the wall, the transformation metrics are calculated as the following

$$(f_\eta)_{i,0} = \frac{-25f_{i,0} + 48f_{i,1} - 36f_{i,2} + 16f_{i,3} - 3f_{i,4}}{12} \quad (15)$$

We calculate the transformation metrics $x_\xi, x_\eta, y_\xi, y_\eta$ with fourth order accuracy $O(\Delta\xi^4, \Delta\eta^4)$ using the 5 point finite difference equations given above. We note that using higher order accuracy for the transformation metrics increases the accuracy of the solution of the governing equations.

For the wall boundary conditions, using the velocity of the moving lid, at the top wall of the arc-shaped cavity the vorticity value is calculated as the following

$$\omega_{i,0} = \frac{\gamma}{J^2} \left(2\psi_{i,1} + 2\frac{J}{x_\xi} \right) \quad (16)$$

Similarly on the bottom curved wall we calculate the vorticity value as the following

$$\omega_{i,0} = 2\frac{\gamma}{J^2} \psi_{i,1} \quad (17)$$

3. RESULTS

Using the numerical procedure described in the previous section we solved the governing flow equations for the wall driven arc-shaped cavity flow problem iteratively. While investigating the sudden dramatic change in the flow topology presented in [Mercan and Atalık \(2009\)](#) for the arc-shaped cavity flow with arc length ratios that are equal to 1/3, 1/4 and 1/5, we discover that the arc-shaped cavity flow has multiple steady solutions at high Reynolds numbers. Multiple steady solutions of the arc-shaped cavity flow exist only when the arc length ratio of the cavity is less than 1/2 (ie. $r < 1/2$). We note that for the $r = 1/2$ case we did not experience multiplicity in steady solutions. However for the $r < 1/2$ cases depending on the initial guess used for the iterative numerical scheme, the iterations converged to different numerical solutions for the same Reynolds numbers above a bifurcation Reynolds number.

As a measure for convergence, during the iterations we monitor the difference in the streamfunction and vorticity variables between two consecutive iteration steps and normalize it by the streamfunction and vorticity value at the previous iteration step as the following

$$residual_{\psi} = \max \left(\frac{|\psi_{i,j}^{k+1} - \psi_{i,j}^k|}{\psi_{i,j}^k} \right)$$

$$residual_{\omega} = \max \left(\frac{|\omega_{i,j}^{k+1} - \omega_{i,j}^k|}{\omega_{i,j}^k} \right) \quad (18)$$

where the superscript shows the iteration step and max denotes the maximum absolute value in the computational domain. In our numerical solutions we carry the iterations until both $residual_{\psi}$ and $residual_{\omega}$ are less than 10^{-6} . This means that in our study we consider the convergence is achieved when the streamfunction and vorticity variables change only one millionth of their values in absolute value between two iteration steps at a grid point as the maximum and in the rest of the grid points the change is even less. This very low convergence limits show that our numerical solutions of the steady arc-shaped cavity flow are indeed very accurate.

In the present study at first we consider the arc-shaped cavity with arc length ratio $r = 1/3$. Using a homogeneous initial guess for the streamfunction (ψ) and vorticity (ω) variables we solve the arc-shaped cavity flow for a low Reynolds number. We use this obtained solution as initial guess and then solve for the next higher Reynolds number repeatedly. By incrementing the Reynolds number each time, we obtain numerical solution of the arc-shaped cavity flow with $r = 1/3$ until Reynolds number of 14000. At higher Reynolds number above 14000, we could not obtain a converged numerical solution. Figure 5 and Fig. 6 show the streamfunction contours of the arc-shaped cavity flow with $r = 1/3$

until $Re = 5000$ and $Re = 14000$ respectively (1^{st} solution) and in Table 1 we tabulate the min and max streamfunction values, their (x, y) locations and the vorticity value at those points.

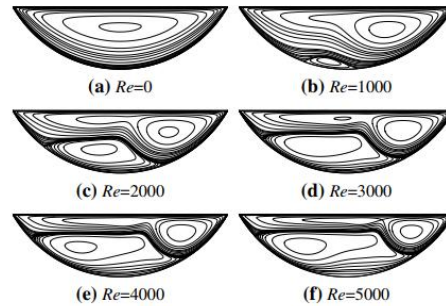


Fig. 4. The 1st solution of arc-shaped cavity flow with $r=1/3$ for various Reynolds numbers until $Re=5000$.

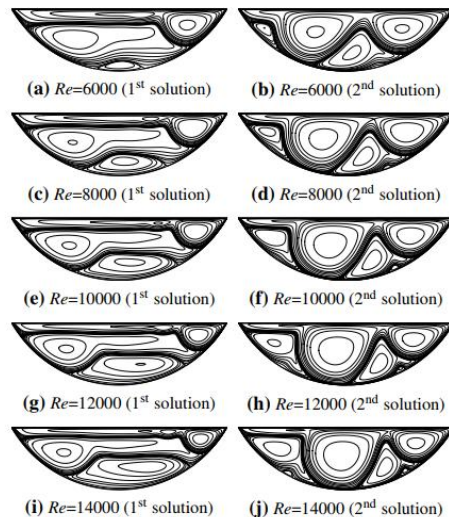


Fig. 5. Multiple solutions of arc-shaped cavity flow with $r=1/3$ for the same Reynolds numbers, the 1st solution on the left, the 2nd solution on the right.

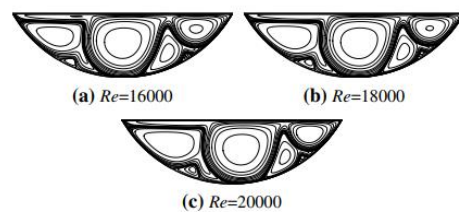


Fig. 6. The 2nd solution of arc-shaped cavity flow with $r=1/3$ for various Reynolds numbers until $Re=20000$.

When we compare our results (1^{st} solution) for arc length ratio $r=1/3$ with that of [Mercan and Atalık \(2009\)](#) we see that at low Reynolds numbers our

Table 1 Minimum and maximum streamfunction, (x,y) location and vorticity for the 1st solution of arc-shaped cavity flow with $r=1/3$.

	Re	x	y	ψ	ω
ψ_{min}	0	0	-0.0924	-4.1542×10^{-2}	7.4518
	1000	0.1857	-0.1053	-4.5034×10^{-2}	8.8656
	2000	0.2235	-0.0981	-4.2288×10^{-2}	9.9186
	3000	0.2575	-0.0904	-3.9251×10^{-2}	11.0364
	4000	0.2827	-0.0840	-3.6681×10^{-2}	12.1025
	5000	0.3011	-0.0789	-3.4529×10^{-2}	13.1118
	6000	0.3160	-0.0745	-3.2697×10^{-2}	14.0757
	8000	0.3374	-0.0678	-2.9750×10^{-2}	15.8986
	10000	0.3537	-0.0623	-2.7454×10^{-2}	17.6355
	12000	0.3667	-0.0578	-2.5590×10^{-2}	19.3300
	14000	0.3779	-0.0537	-2.4037×10^{-2}	21.0060
ψ_{max}	1000	-0.0818	-0.2515	9.9563×10^{-5}	-0.5722
	2000	-0.0981	-0.1785	3.0539×10^{-3}	-1.9139
	3000	-0.1631	-0.1592	4.6093×10^{-3}	-2.4042
	4000	-0.1914	-0.1502	5.8028×10^{-3}	-2.6467
	5000	-0.1979	-0.1460	6.6096×10^{-3}	-2.6803
	6000	-0.2026	-0.1423	7.1036×10^{-3}	-2.7127
	8000	-0.2155	-0.1340	7.6210×10^{-3}	-2.8372
	10000	-0.2323	-0.1270	7.8357×10^{-3}	-2.9656
	12000	-0.2455	-0.1209	7.8992×10^{-3}	-3.0866
	14000	-0.2569	-0.1153	7.8922×10^{-3}	-3.2006

results agree well with each other, however at high Reynolds numbers our results are not even close with that of [Mercan and Atalik \(2009\)](#). For example for $Re=8000$, the streamfunction contours shown in Fig. 5c is completely different than the same in [Mercan and Atalik \(2009\)](#) to the point as if they are two different flow problems. While trying to figure out the reason for this, by coincidence we start a numerical iteration at a high Reynolds number using a homogeneous initial guess for both the streamfunction (ψ) and vorticity (ω) variables instead of using the previous smaller Reynolds number solution. When we obtain the numerical solution we see that for the considered Reynolds number this time we obtain a completely different solution which looks very similar to the solutions of [Mercan and Atalik \(2009\)](#) at high Reynolds numbers. After many repeated runs we find out that at a given Reynolds number the flow problem at hand, the arc-shaped cavity flow, has two different steady state solutions at high Reynolds numbers. After this discovery of the multiplicity of steady state solutions in arc-shaped cavity flow, in order to obtain the whole Reynolds number range for this newly found second solution we used this obtained second solution as initial guess and increment the Reynolds number to higher and also lower values. In Fig. 5 and Fig. 6, we present the streamfunction contours of the newly found second solution of the arc-shaped cavity flow with $r=1/3$ until $Re=14000$ and $Re=20000$ respectively (2nd solution). Also for this second solution in Table 2.

we tabulate the min and max streamfunction values, their (x,y) locations and the vorticity value at those points. When we compare our 2nd solutions with the solutions of [Mercan and Atalik \(2009\)](#) at high Reynolds numbers we see that they agree well with each other. At this point it was clear that, with out realizing that the arc-shaped cavity flow have multiple steady state solutions, [Mercan and Atalik \(2009\)](#) have presented mixed results of 1st solutions and 2nd solutions at different Reynolds numbers (ie. 1st solutions at low Reynolds numbers and 2nd solutions at high Reynolds numbers).

At low Reynolds numbers when we tried several different initial guesses, we consistently obtain the 1st solutions only. Hence at low Reynolds numbers, we find only one solution for any considered Reynolds number and in this study we refer to this solutions as the "1st solutions". At high Reynolds numbers we obtain a second set of solutions and we refer to this new solutions as the "2nd solutions". In order to see the differences of these two solutions better, in Fig. 5 we plot the streamfunction contours of the two solutions for the same particular Reynolds numbers next to each other.

For the considered case of the arc-shaped driven cavity with arc length ratio $r=1/3$, in order to obtain the bifurcation Reynolds number that the flow starts to have multiple solutions we consider many runs with incrementing or decrementing the Reynolds

Table 2 Minimum and maximum streamfunction, (x,y) location and vorticity for the 2nd solution of arc-shaped cavity flow with r=1/3.

	Re	x	y	ψ	ω
ψ_{min}	5164	0.2512	-0.0942	-4.2377×10^{-2}	11.2622
	6000	0.2597	-0.0921	-4.1610×10^{-2}	11.6453
	8000	0.2816	-0.0864	-3.9327×10^{-2}	12.6297
	10000	0.2983	-0.0817	-3.7212×10^{-2}	13.5900
	12000	-0.0480	-0.1288	-3.7822×10^{-2}	6.1817
	14000	-0.0213	-0.1297	-3.8519×10^{-2}	6.1862
	16000	0.0018	-0.1328	-3.8895×10^{-2}	6.2150
	18000	0.0232	-0.1325	-3.9045×10^{-2}	6.2610
	20000	0.0428	-0.1319	-3.9019×10^{-2}	6.3205
ψ_{max}	5164	-0.0059	-0.2078	5.2560×10^{-3}	-3.3184
	6000	0.0331	0.2042	5.7674×10^{-3}	-3.4533
	8000	0.0873	0.1996	6.3444×10^{-3}	-3.9145
	10000	0.1255	-0.1938	6.5677×10^{-3}	-4.3554
	12000	0.1577	-0.1873	6.6066×10^{-3}	-4.7802
	14000	0.1837	-0.1809	6.5386×10^{-3}	-5.1849
	16000	0.2065	-0.1769	6.4080×10^{-3}	-5.5772
	18000	0.2246	-0.1711	6.2388×10^{-3}	-5.9695
	20000	0.2426	-0.1648	6.0429×10^{-3}	-6.3560

number by only 1. We note that as seen in Fig. 4 below Reynolds number of 5000 we obtain only the 1st solution. Also by using the previous smaller Reynolds number solution as initial guess and we were able to obtain the 1nd solution until Reynolds number of 14000 as seen in Fig. 5 even though the 2nd solution exist above Re = 6000 also as seen in Fig. 5. Therefore the bifurcation Reynolds number for having multiple steady solution must be in the range between Re = 5000 and Re = 6000. In order to pinpoint the exact bifurcation Reynolds number we used two different approaches. As mentioned above, we obtain the second solution when we used a homogeneous initial guess for the iterative numerical scheme at high Reynolds numbers. Therefore as the first approach, we use a homogeneous initial guess for the streamfunction (ψ) and vorticity (ω) variables each time and run many cases with incrementing the Reynolds number between Re = 5000 and Re = 6000. With using a homogeneous initial guess we find that while at

Re = 5163 we obtain the 1st solution as the converged solution, at exactly Re = 5164 we start to obtain the 2nd solution as the converged solution. The streamfunction contours for the obtained the 1st solution at Re = 5163 and the 2nd solution at Re = 5164 are given in Fig. 7. Also as mentioned above, no matter how different initial guesses we used for the iterative numerical scheme, at low Reynolds numbers the only obtained numerical solution is the 1st solution. Therefore as the second approach, which also works as a check to our finding of the first approach, we used the 2nd solution

obtained at Re = 5164 given in Fig. 7b as the initial guess and we run for Re = 5163. Since below the bifurcation Reynolds numbers there exist only the 1st solution, in this exercise we expected to obtain the 1st solution at Re = 5163 even though we used the 2nd solution obtained at Re = 5164 as an initial guess. In this exercise, as expected, we see that at the convergence we obtain the 1st solution seen in Fig. 7a. After applying these two approaches one after the other, we find that for the arc-shaped cavity flow with arc length ratio r=1/3 the bifurcation Reynolds number for having multiple steady solutions is Re = 5164. Above Re = 5164 there exist two different steady solutions until the highest Reynolds number of 14000 for the 1nd solution. Above Re = 14000 we obtain only the the 2nd solution until Re = 20000 which is the highest Reynolds number we can obtain for the 2nd solution.

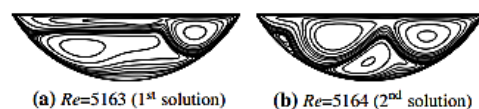


Fig. 7. Solutions of arc-shaped cavity flow with r=1/3 at the bifurcation Reynolds number.

We note that for both the 1st solution and the 2nd solution, away from the bifurcation Reynolds number the convergence is monotonic and rather fast for example when a previous smaller Reynolds number solution of the 1st solution is used as a guess

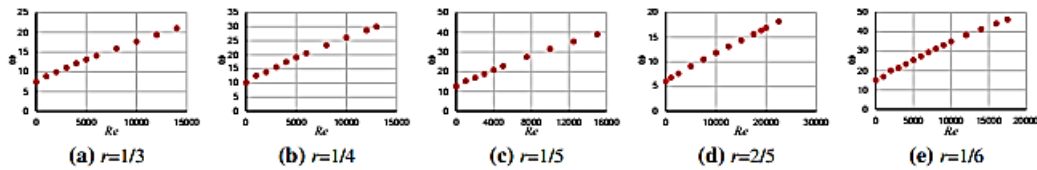


Fig. 8. Variation of vorticity at the point of minimum streamfunction for the 1st solution.

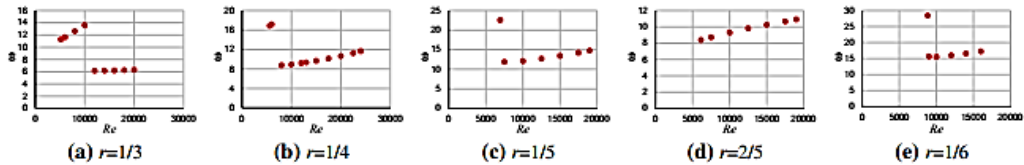


Fig. 9. Variation of vorticity at the point of minimum streamfunction for the 2nd solution.

solution. The same is also true for the 2nd solution. However, as also mentioned earlier, if the 2nd solution is used as an initial guess for Reynolds number below the bifurcation Reynolds number at which there exist only the 1st solution, the convergence is very slow and not monotonic. In this case at first the iterations starts to convergence up to some level but then the residuals starts to increase for some iterations after which the residuals then starts to decrease monotonically to full convergence. For this reason in arc-shaped cavity flow the convergence limit must be low enough to guarantee that the final converged steady state is achieved.

In Fig. 8a we plot the vorticity at the min streamfunction point as a function of the Reynolds number for the 1st solution that is tabulated in Table 1. In Fig. 8a after seeing the linear behavior of the vorticity with respect to the Reynolds number, we decided to include the limiting case of the Stokes flow, ie. $Re = 0$, to our analysis in order to see if this linear behavior goes all the way down to $Re = 0$ and we solve the arc-shaped cavity flow for $Re = 0$. As seen in Fig. 8a, for the 1st solution the vorticity at the core of the primary vortex (the first vortex at the very top closest to the lid of the arc shape cavity) increases almost linearly as the Reynolds number increases all in the range from $Re = 0$ to $Re = 14000$.

Similarly, in Fig. 9a we plot the vorticity at the min streamfunction point as a function of the Reynolds number for the 2nd solution that is tabulated in Table 2. In Fig. 9a we can see that between $Re = 5164$ and $Re = 10000$ the vorticity increases almost linearly. However, at $Re = 12000$ there is a sudden decrease in the vorticity and as the Reynolds number increases further between $Re = 12000$ and $Re = 20000$ the vorticity slightly increases linearly.

In streamfunction contours of the 2nd solution in Fig. 5 we can see that there are two local centers in the biggest top vortex closest to the lid, one towards

the top right corner of the arc-shaped cavity and one towards slightly the left of the mid of the arc-shaped cavity. When we examine the x and y location of the minimum streamfunction point given in Table 2 and trace this point in the contour figures of the 2nd solution in Fig 5, we see that between $Re = 5164$ and $Re = 10000$ the location of the minimum streamfunction point coincides with the local minima towards top right corner of the the first vortex at the very top closest to the lid. However the location of the minimum streamfunction point shifts to the other local minima towards slightly the left of the mid of the closest vortex to the lid between $Re = 12000$ and $Re = 20000$.

In Fig. 10a and Fig. 11a we do the same and plot the vorticity at max streamfunction point as a function of the Reynolds number both for the 1st solution and the 2nd solution respectively. In Fig. 10a we see that for the 1st solution the max streamfunction point coincides with the secondary vortex throughout the whole Reynolds number range. Also, for the 2nd solution in Fig. 11a, we see that the max streamfunction point do not shift vortices and the vorticity at this location increases (in absolute value) almost linearly with respect to the Reynolds number.

When we examine the 1st solution of the arc-shaped cavity flow with arc length ratio $r = 1/3$ in Fig. 4, Fig. 5 and Fig. 7, we see the appearance of a new secondary vortex between $Re = 0$ and $Re = 10000$ and a new tertiary vortex between $Re = 5163$ and $Re = 6000$ in the flow field and the size of these vortices grow bigger as the Reynolds number increases. At the highest Reynolds number of 14000 there are three vortices in the flow field in the 1nd solution. On the other hand, when we examine the 2nd solution of the arc-shaped cavity flow with arc length ratio $r = 1/3$ in Fig. 5, Fig. 6 and Fig. 7, we see that the 2nd solution has three vortices at the

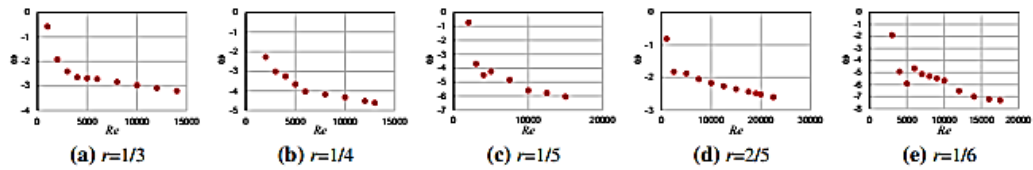


Fig. 10. Variation of vorticity at the point of maximum streamfunction for the 1st solution.

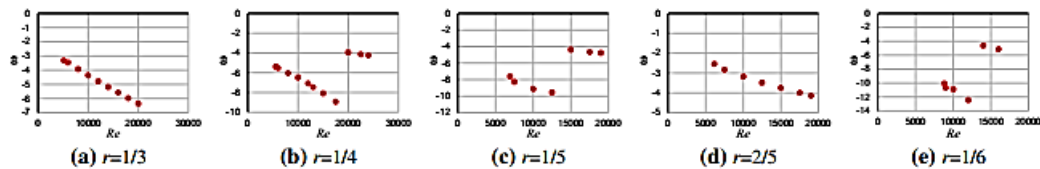


Fig. 11. Variation of vorticity at the point of maximum streamfunction for the 2nd solution.

bifurcation Reynolds number of $Re = 5164$. Between $Re = 6000$ and $Re = 8000$ a new quaternary vortex and also between $Re = 12000$ and $Re = 14000$ a new quinary vortex appear in the flow field. At the highest Reynolds number of 20000 there are five vortices in the flow field in the 2nd solution.

bifurcation Reynolds numbers for the considered arc length ratios. The similar figures and also tables for the arc length ratios $r=1/4$, $1/5$, $2/5$ and also $1/6$ are given in Fig. 12 to Fig. 27 and in Table 3 to Table 10.

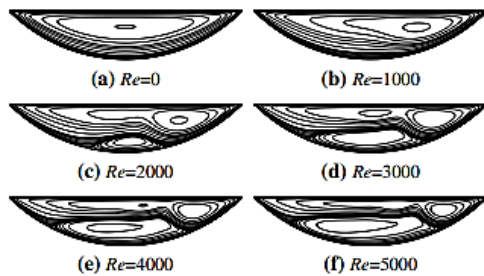


Fig. 12. The 1st solution of arc-shaped cavity flow with $r=1/4$ for various Reynolds numbers until $Re=5000$.

We carry the same analysis to the arc-shaped cavity flow with arc length ratio $r=1/4$, $1/5$, $2/5$ and also $1/6$. Following the same procedure, in all these cases we first obtain the 1st solution by considering a low Reynolds number. Then using this smaller Reynolds number as an initial guess for the next higher Reynolds number we obtain the 1st solution of the arc-shaped cavity flow until the highest Reynolds number we can obtain. Then using a homogeneous initial condition we solve for a high Reynolds number and obtain the 2nd solution at the considered Reynolds number. Then again using the previous Reynolds number solution as initial guess we obtain the 2nd solution the whole Reynolds number range by incrementing or decrementing the Reynolds number. Finally we follow the two approaches described above for finding the bifurcation Reynolds number and we obtain the

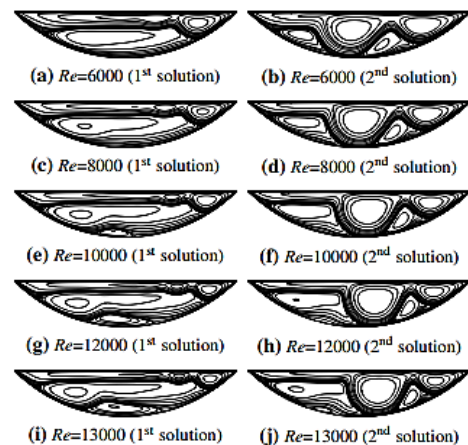


Fig. 13. Multiple solutions of arc-shaped cavity flow with $r=1/4$ for the same Reynolds numbers, the 1st solution on the left, the 2nd solution on the right.

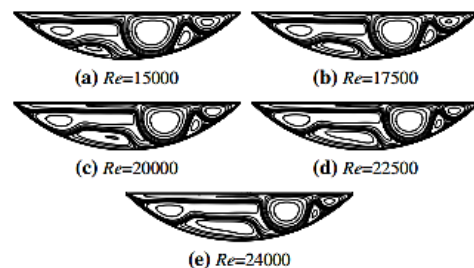


Fig. 14. The 2nd solution of arc-shaped cavity flow with $r=1/4$ for various Reynolds numbers until $Re=24000$.

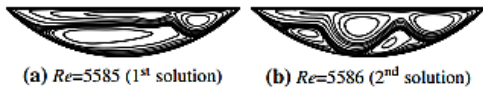


Fig. 15. Solutions of arc-shaped cavity flow with $r=1/4$ at the bifurcation Reynolds number.

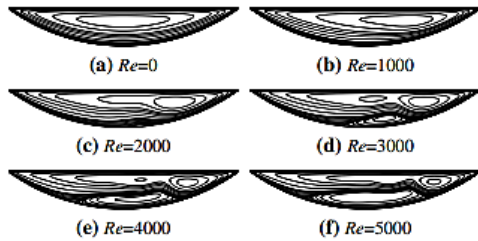


Fig. 16. The 1st solution of arc-shaped cavity flow with $r=1/5$ for various Reynolds numbers until $Re=5000$.

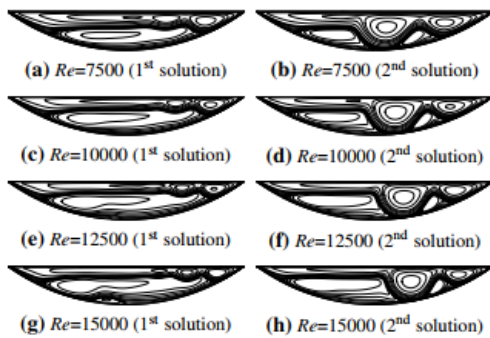


Fig. 17. Multiple solutions of arc-shaped cavity flow with $r=1/5$ for the same Reynolds numbers, the 1st solution on the left, the 2nd solution on the right.



Fig. 18. The 2nd solution of arc-shaped cavity flow with $r=1/5$ for various Reynolds numbers until $Re=19000$.

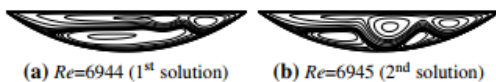


Fig. 19. Solutions of arc-shaped cavity flow with $r=1/5$ at the bifurcation Reynolds number.

For the arc length ratio $r=1/4$, in Fig. 12 and Fig. 13 we can see that between $Re=1000$ and $Re=2000$ a secondary vortex and between $Re=8000$ and

$Re=10000$ a tertiary vortex appear in the flow. At the highest Reynolds number of 13000 for the 1st solution, there are three vortices in the flow field. For the considered $r=1/4$ case the bifurcation Reynolds number at which a second solution start to exist is $Re=5586$. At this bifurcation Reynolds number of $Re=5586$, the 2nd solution has three vortex in the flow field as seen in Fig. 15. Also as seen in Fig. 13 between $Re=8000$ and $Re=10000$ and also between $Re=10000$ and $Re=12000$, a new quaternary and a new quinary vortex appear in the 2nd solution respectively.

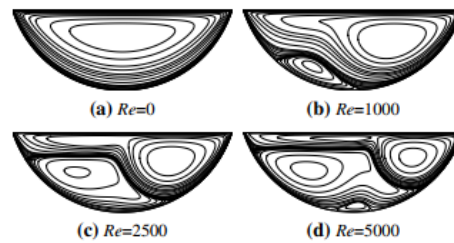


Fig. 20. The 1st solution of arc-shaped cavity flow with $r=2/5$ for various Reynolds numbers until $Re=5000$.

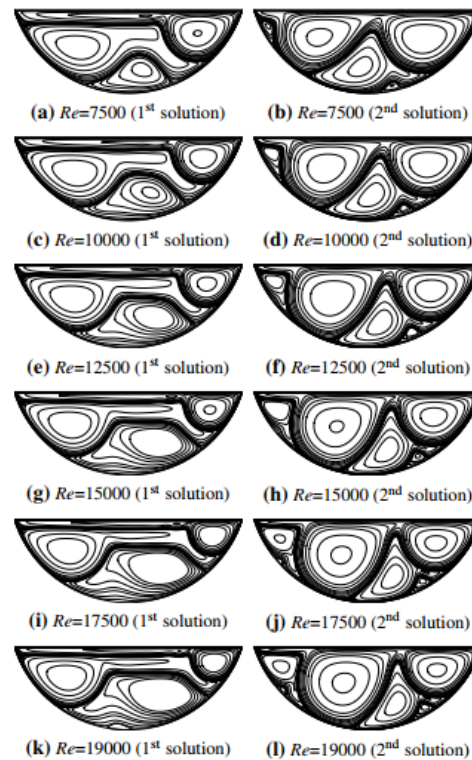


Fig. 21. Multiple solutions of arc-shaped cavity flow with $r=2/5$ for the same Reynolds numbers, the 1st solution on the left, the 2nd solution on the right.

From Fig. 16 and Fig. 17, in the arc-shaped cavity flow with arc length ratio $r=1/5$, a secondary vortex

Table 3 Minimum and maximum streamfunction, (x,y) location and vorticity for the 1st solution of arc-shaped cavity flow with r=1/4.

	Re	x	y	ψ	ω
ψ_{min}	0	0	-0.0673	-3.0218×10^{-2}	10.0828
	1000	0.1995	-0.0700	-3.2001×10^{-2}	12.6458
	2000	0.2288	-0.0700	-3.1320×10^{-2}	13.8672
	3000	0.2642	-0.0640	-2.9161×10^{-2}	15.6821
	4000	0.2909	-0.0588	-2.7093×10^{-2}	17.4335
	5000	0.3109	-0.0546	-2.5374×10^{-2}	19.0628
	6000	0.3258	-0.0513	-2.3947×10^{-2}	20.5934
	8000	0.3472	-0.0463	-2.1709×10^{-2}	23.4419
	10000	0.3636	-0.0421	-1.9996×10^{-2}	26.1202
	12000	0.3767	-0.0387	-1.8631×10^{-2}	28.6897
	13000	0.3816	-0.0374	-1.8045×10^{-2}	29.9527
ψ_{max}	2000	0.0220	-0.1576	8.5702×10^{-4}	-2.2739
	3000	0.0144	-0.1423	2.1066×10^{-3}	-3.0125
	4000	-0.0839	-0.1311	3.0091×10^{-3}	-3.2552
	5000	-0.1331	-0.1232	3.6872×10^{-3}	-3.6617
	6000	-0.1665	-0.1183	4.2985×10^{-3}	-4.0331
	8000	-0.1831	-0.1108	5.1924×10^{-3}	-4.1780
	10000	-0.1982	-0.1057	5.6219×10^{-3}	-4.3254
	12000	-0.2133	-0.1006	5.8276×10^{-3}	-4.5170
	13000	-0.2218	-0.0988	5.8771×10^{-3}	-4.6118

Table 4. Minimum and maximum streamfunction, (x,y) location and vorticity for the 2nd solution of arc-shaped cavity flow with r=1/4.

	Re	x	y	ψ	ω
ψ_{min}	5586	0.2762	-0.0636	-2.9725×10^{-2}	16.8789
	6000	0.2796	-0.0629	-2.9489×10^{-2}	17.1660
	8000	0.0052	-0.0880	-2.8674×10^{-2}	8.7708
	10000	0.0396	-0.0901	-2.9425×10^{-2}	8.9493
	12000	0.0705	-0.0889	-2.9629×10^{-2}	9.2088
	13000	0.0844	-0.0906	-2.9607×10^{-2}	9.3569
	15000	0.1102	-0.0888	-2.9381×10^{-2}	9.6817
	17500	0.1393	-0.0862	-2.8856×10^{-2}	10.1397
	20000	0.1667	-0.0832	-2.8139×10^{-2}	10.6613
	22500	0.1922	-0.0798	-2.7276×10^{-2}	11.2593
	24000	0.2075	-0.0776	-2.6701×10^{-2}	11.6612
	ψ_{max}	5586	0.0893	-0.1508	2.8595×10^{-3}
6000		0.1020	-0.1494	2.9936×10^{-3}	-5.5153
8000		0.1506	-0.1424	3.3821×10^{-3}	-6.0370
10000		0.1909	-0.1321	3.5723×10^{-3}	-6.4737
12000		0.2219	-0.1226	3.6279×10^{-3}	-7.0829
13000		0.2357	-0.1190	3.6193×10^{-3}	-7.4472
15000		0.2580	-0.1127	3.5556×10^{-3}	-8.0853
17500		0.2818	-0.1053	3.4108×10^{-3}	-8.9290
20000		-0.2919	-0.0782	3.4525×10^{-3}	-3.9395
22500		-0.2986	-0.0764	3.5784×10^{-3}	-4.1337
24000		-0.3036	-0.0750	3.6385×10^{-3}	-4.2390

Table 5 Minimum and maximum streamfunction, (x,y) location and vorticity for the 1st solution of arc-shaped cavity flow with $r=1/5$.

	Re	x	y	ψ	ω
ψ_{min}	0	0	-0.0534	-2.3842×10^{-2}	12.6328
	1000	0.1909	-0.0537	-2.4137×10^{-2}	15.2657
	2000	0.2198	-0.0545	-2.5217×10^{-2}	16.9258
	3000	0.2503	-0.0524	-2.4261×10^{-2}	18.8088
	4000	0.2770	-0.0485	-2.2810×10^{-2}	20.8833
	5000	0.2987	-0.0451	-2.1405×10^{-2}	22.9024
	7500	0.3352	-0.0387	-1.8688×10^{-2}	27.4936
	10000	0.3567	-0.0345	-1.6835×10^{-2}	31.5609
	12500	0.3732	-0.0312	-1.5480×10^{-2}	35.3036
	15000	0.3847	-0.0287	-1.4435×10^{-2}	38.8404
ψ_{max}	2000	0.0784	-0.1520	5.5525×10^{-6}	-0.7189
	3000	0.0902	-0.1215	7.0950×10^{-4}	-3.6741
	4000	0.1019	-0.1137	1.3207×10^{-3}	-4.4901
	5000	-0.0175	-0.1090	1.9044×10^{-3}	-4.2352
	7500	-0.1180	-0.0989	2.9394×10^{-3}	-4.8204
	10000	-0.1680	-0.0931	3.8089×10^{-3}	-5.5957
	12500	-0.1814	-0.0892	4.3583×10^{-3}	-5.7780
	15000	-0.1947	-0.0852	4.6365×10^{-3}	-6.0381

Table 6. Minimum and maximum streamfunction, (x,y) location and vorticity for the 2nd solution of arc-shaped cavity flow with $r=1/5$.

	Re	x	y	ψ	ω
ψ_{min}	6945	0.2904	-0.0464	-2.2744×10^{-2}	22.5838
	7500	0.0491	-0.0644	-2.2521×10^{-2}	11.8725
	10000	0.0883	-0.0675	-2.3468×10^{-2}	12.1201
	12500	0.1222	-0.0655	-2.3509×10^{-2}	12.7157
	15000	0.1528	-0.0653	-2.3192×10^{-2}	13.4213
	17500	0.1815	-0.0626	-2.2662×10^{-2}	14.2178
	19000	0.1967	-0.0610	-2.2274×10^{-2}	14.7466
ψ_{max}	6945	0.1495	-0.1126	1.8541×10^{-3}	-7.6052
	7500	0.1568	-0.1137	1.9361×10^{-3}	-8.2628
	10000	0.2001	-0.1063	2.1528×10^{-3}	-9.1175
	12500	0.2357	-0.0969	2.2505×10^{-3}	-9.5373
	15000	-0.2456	-0.0764	2.4321×10^{-3}	-4.3740
	17500	-0.2523	-0.0751	2.7238×10^{-3}	-4.6455
	19000	-0.2554	-0.0727	2.8517×10^{-3}	-4.7662



Fig. 22. The 1st solution of arc-shaped cavity flow with $r=2/5$ for various Reynolds numbers until $Re=22500$.

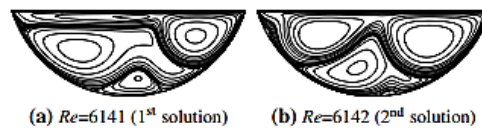


Fig. 23. Solutions of arc-shaped cavity flow with $r=2/5$ at the bifurcation Reynolds number.

Table 7. Minimum and maximum streamfunction, (x,y) location and vorticity for the 1st solution of arc-shaped cavity flow with r=2/5.

	Re	x	y	ψ	ω
ψ_{min}	0	0	-0.1156	-5.1450×10^{-2}	6.0464
	1000	0.1625	-0.1371	-5.6629×10^{-2}	6.7954
	2500	0.2159	-0.1284	-5.2138×10^{-2}	7.6374
	5000	0.2710	-0.1126	-4.5527×10^{-2}	9.1007
	7500	0.3056	-0.0984	-4.0548×10^{-2}	10.5284
	10000	0.3286	-0.0897	-3.6898×10^{-2}	11.8465
	12500	0.3465	-0.0824	-3.4038×10^{-2}	13.1132
	15000	0.3587	-0.0754	-3.1697×10^{-2}	14.3658
	17500	0.3699	-0.0706	-2.9735×10^{-2}	15.6174
	19000	0.3762	-0.0677	-2.8697×10^{-2}	16.3759
	20000	0.3794	-0.0663	-2.8052×10^{-2}	16.8873
	22500	0.3872	-0.0627	-2.6578×10^{-2}	18.1949
ψ_{max}	1000	-0.1867	-0.2533	6.2296×10^{-4}	-0.8088
	2500	-0.2137	-0.1807	5.4303×10^{-3}	-1.8247
	5000	-0.1958	-0.1744	8.7170×10^{-3}	-1.8739
	7500	-0.2134	-0.1605	9.5825×10^{-3}	-2.0507
	10000	-0.2286	-0.1530	1.0063×10^{-2}	-2.1632
	12500	-0.2401	-0.1464	1.0262×10^{-2}	-2.2619
	15000	-0.2524	-0.1423	1.0276×10^{-2}	-2.3532
	17500	-0.2619	-0.1363	1.0213×10^{-2}	2.4388
	19000	-0.2688	-0.1338	1.0148×10^{-2}	-2.4887
	20000	-0.2722	-0.1325	1.0097×10^{-2}	-2.5215
	22500	-0.2799	-0.1271	9.9511×10^{-3}	-2.6023

Table 8. Minimum and maximum streamfunction, (x,y) location and vorticity for the 2nd solution of arc-shaped cavity flow with r=2/5.

	Re	x	y	ψ	ω
ψ_{min}	6142	0.2340	-0.1264	-5.3548×10^{-2}	8.4037
	7500	0.2444	-0.1234	-5.2284×10^{-2}	8.7328
	10000	0.2625	-0.1153	-4.9803×10^{-2}	9.3038
	12500	0.2761	-0.1109	-4.7617×10^{-2}	9.8102
	15000	0.2879	-0.1069	-4.5723×10^{-2}	10.2642
	17500	0.2980	-0.1034	-4.4073×10^{-2}	10.6782
	19000	0.3030	-0.1016	-4.3177×10^{-2}	10.9120
ψ_{max}	6142	-0.0659	-0.2409	8.1185×10^{-3}	-2.5398
	7500	-0.0270	-0.2471	8.7970×10^{-3}	-2.8206
	10000	0.0209	-0.2506	9.3554×10^{-3}	-3.1800
	12500	0.0568	-0.2550	9.5589×10^{-3}	-3.4845
	15000	0.0881	-0.2512	9.5823×10^{-3}	-3.7539
	17500	0.1114	-0.2506	9.5084×10^{-3}	-3.9993
	19000	0.1244	-0.2513	9.4323×10^{-3}	-4.1368

and also a tertiary vortex appear in the 1nd solution between Re=1000 and Re=2000 and Re=1000 and Re=12500 respectively. The highest Reynolds number we can obtain for the 1nd solution is Re=15000 and at this Reynold number there are three vortices in the 1nd solution flow field. For r=1/5 case, we find the bifurcation point for multiple steady

solutions is Re=6945 as shown in Fig. 19. At this bifurcation Reynolds number there are three vortices in the flow field. Between Re=12500 and Re=15000 and also between Re=15000 and Re=17500 we see the appearance of a new quaternary and a new quinary vortex respectively in the 2nd solution as seen in Fig. 17 and Fig. 18.

Table 9. Minimum and maximum streamfunction, (x,y) location and vorticity for the 1st solution of arc-shaped cavity flow with r=1/6.

	Re	x	y	ψ	ω
ψ_{min}	0	0	-0.0447	-1.9719×10^{-2}	15.0471
	1000	0.1478	-0.0428	-1.9525×10^{-2}	16.8701
	2000	0.2170	-0.0436	-2.0547×10^{-2}	20.0794
	3000	0.2356	-0.0435	-2.0670×10^{-2}	21.4076
	4000	0.2575	-0.0428	-2.0026×10^{-2}	23.3764
	5000	0.2792	-0.0401	-1.9091×10^{-2}	25.4007
	6000	0.2976	-0.0377	-1.8116×10^{-2}	27.4641
	7000	0.3126	-0.0356	-1.7216×10^{-2}	29.4698
	8000	0.3259	-0.0336	-1.6416×10^{-2}	31.3991
	9000	0.3358	-0.0321	-1.5713×10^{-2}	33.2479
	10000	0.3458	-0.0305	-1.5097×10^{-2}	35.0261
	12000	0.3590	-0.0283	-1.4080×10^{-2}	38.3504
	14000	0.3706	-0.0264	-1.3277×10^{-2}	41.4335
	16000	0.3788	-0.0249	-1.2621×10^{-2}	44.3365
	17500	0.3838	-0.0240	-1.2201×10^{-2}	46.4278
ψ_{max}	3000	0.1128	-0.1169	4.3233×10^{-3}	-1.8707
	4000	0.1286	-0.1004	4.6536×10^{-3}	-4.9141
	5000	0.1471	-0.0941	8.2788×10^{-3}	-5.9210
	6000	0.0138	-0.0959	1.0912×10^{-3}	-4.6476
	7000	0.0155	-0.0915	1.5419×10^{-3}	-5.1355
	8000	0.0017	-0.0893	1.8307×10^{-3}	-5.3061
	9000	-0.0481	-0.0863	2.0886×10^{-3}	-5.4592
	10000	-0.0668	-0.0834	2.3054×10^{-3}	-5.6593
	12000	-0.1456	-0.0799	2.7221×10^{-3}	-6.5139
	14000	-0.1643	-0.0779	3.1599×10^{-3}	-6.9936
	16000	-0.1728	-0.0769	3.4761×10^{-3}	-7.2096
17500	-0.1777	-0.0744	3.6382×10^{-3}	-7.2941	

Table 10. Minimum and maximum streamfunction, (x,y) location and vorticity for the 2nd solution of arc-shaped cavity flow with r=1/6.

	Re	x	y	ψ	ω
ψ_{min}	8825	0.3026	-0.0370	-1.8311×10^{-2}	28.4075
	9000	0.1011	-0.0514	-1.8591×10^{-2}	15.7154
	10000	0.1113	-0.0531	-1.9079×10^{-2}	15.5421
	12000	0.1349	-0.0518	-1.9339×10^{-2}	15.9444
	14000	0.1569	-0.0524	-1.9276×10^{-2}	16.5593
	16000	0.1771	-0.0509	-1.9060×10^{-2}	17.2580
ψ_{max}	8825	0.1883	-0.0887	1.3152×10^{-3}	-10.0619
	9000	0.1869	-0.0908	1.3334×10^{-3}	-10.6963
	10000	0.2005	-0.0887	1.4018×10^{-3}	-10.8898
	12000	0.2227	-0.0849	1.4909×10^{-3}	-12.4440
	14000	-0.1896	-0.0729	1.6217×10^{-3}	-4.6041
	16000	-0.2116	-0.0700	1.8660×10^{-3}	-5.1375

When we look at Fig. 20, Fig. 21 and Fig. 22 for the arc length ratio $r=2/5$ case, we see that a secondary, a tertiary and a quaternary vortex appear in the 1st solution between $Re=0$ and $Re=1000$, between $Re=2500$ and $Re=5000$ and between $Re=17500$ and $Re=19000$ respectively. At the highest Reynolds

number of $Re=22500$ for the 1st solution of $r=2/5$ case, there are four vortices in the flow field. We find the bifurcation Reynolds number for the $r=2/5$ case as $Re=6142$ where there are four vortices in the flow field of the 2nd solution. Between $Re=12500$ and

Re=15000 a quinary vortex appear in the 2nd solution, and at the highest Reynolds number of 19000 for the 2nd solution the flow has five vortices.

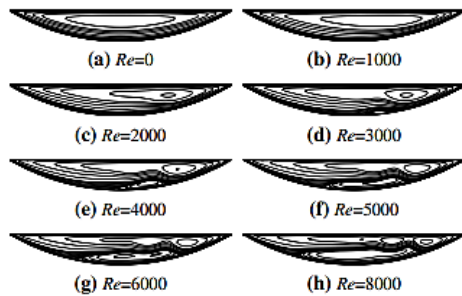


Fig. 24. The 1st solution of arc-shaped cavity flow with $r=1/6$ for various Reynolds numbers until $Re=8000$.

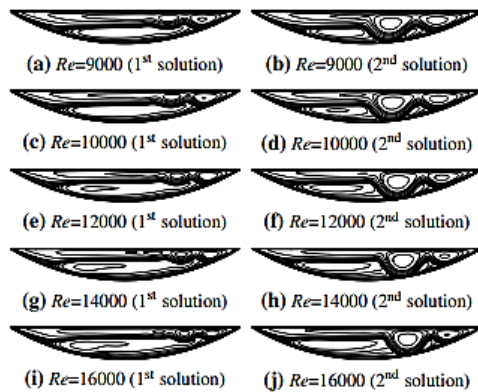


Fig. 25. Multiple solutions of arc-shaped cavity flow with $r=1/6$ for the same Reynolds numbers, the 1st solution on the left, the 2nd solution on the right.



Fig. 26. The 1st solution of arc-shaped cavity flow with $r=1/6$ at $Re=17500$.

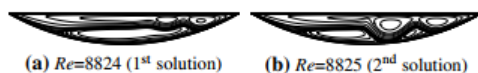


Fig. 27. Solutions of arc-shaped cavity flow with $r=1/6$ at the bifurcation Reynolds number.

Finally in the flow field of the arc-shaped cavity with arc length ratio $r=1/6$, as seen in Fig. 24, Fig. 25 and Fig. 26, a secondary vortex appear between $Re=2000$ and $Re=3000$ and also a tertiary vortex appear between $Re=16000$ and $Re=17500$. The 1st solution has three vortices in the flow field at the highest

Reynolds number of 17500. For $r=1/6$ arc length ratio case, the bifurcation Reynolds number for existence of a second set of solution is 8825 as seen in Fig. 27 and at this Reynolds number the 2nd solution has three vortices in the flow field. At the highest Reynolds number of 16000, there are still three vortices in the flow field of the 2nd solution.

When we look at Fig. 8, we see that for all the arc length ratios considered (ie. $r=1/3, 1/4, 1/5, 2/5$ and $1/6$) in the 1st solution, at the minimum streamfunction location the vorticity increases almost linearly with respect to the Reynolds number from the Stokes regime ($Re=0$) to the maximum obtained Reynolds number.

In Fig. 9 we see that in the 2nd solution, except at $r=2/5$, the location of the minimum streamfunction point shifts from one local minima to another local minima. In the 2nd solution, as seen in Fig. 11, we see that the location of the maximum streamfunction shifts also for the smaller arc length ratios (ie. $r=1/6, 1/5$ and $1/4$). However, the shift in the maximum streamfunction location is different than the shift we see in the minimum streamfunction location. The shift in the minimum streamfunction location occurs in the primary vortex in which the flow rotates in clockwise direction and the shift occurs from one local minima to the other local minima. On the other hand the shift in maximum streamfunction location occurs from one counterrotating vortex on the right bottom side of the arcshaped cavity to the other counter-rotating vortex on the left bottom side of the arc-shaped cavity. When the arc length ratio is high (ie. $r=2/5$ and $1/3$) the maximum streamfunction location always coincides with the center of the counter-rotating vortex on the right bottom side of the arc-shaped cavity for the whole range of the Reynolds number considered.

In our numerical solutions, as the arc length ratio of the arc-shaped cavity changes the highest Reynolds number we can obtain a numerical solution for the 1st solution and also for the 2nd solution change. The bifurcation Reynolds number at which multiple solutions start to exist also changes as the arc length ratio changes. The bar charts Fig. 28, Fig. 29 and Fig. 30 show the variation of the highest Reynolds number that we can obtain a numerical solution for the 1st solution and for the 2nd solution and also the bifurcation Reynolds number as a function of the arc length ratio respectively. As shown in Fig. 28, the highest Reynolds number that we can achieve a numerical solution for the 1st solution first decreases and then increases as the arc length ratio decreases from $r=2/5$ to $r=1/6$ where the minimum is at $r=1/4$. The highest Reynolds number that we can achieve a numerical solution for the 2nd solution shows an opposite behaviour and first increases with having the maximum at $r=1/4$ then decreases as the arc length ratio decreases from $r=2/5$ to $r=1/6$ as given in Fig. 29. Finally, in Fig. 30 we can see that the bifurcation Reynolds number first decreases and then increases as the arc length ratio decreases from $r=2/5$ to $r=1/6$ having the minimum bifurcation Reynolds number at $r=1/3$ arc length ratio.

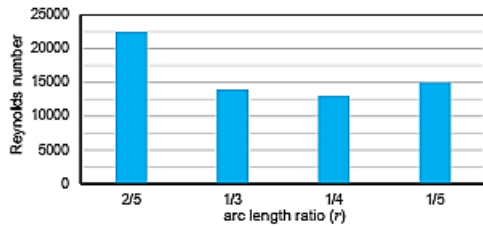


Fig. 28. Highest achieved Reynolds number for the 1st solution of the arc-shaped cavity flow.

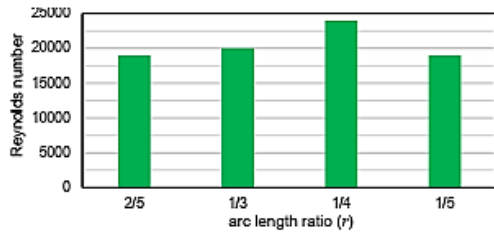


Fig. 29. Highest achieved Reynolds number for the 2nd solution of the arc-shaped cavity flow.

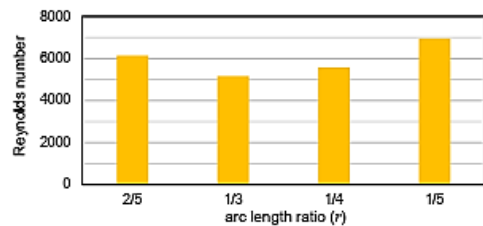


Fig. 30. Bifurcation Reynolds number of the arc-shaped cavity flow.

CONCLUSIONS

In this study steady two-dimensional incompressible viscous flow inside a wall driven arc-shaped cavity is analyzed numerically. Using a body fitted mesh obtained by a conformal mapping, the numerical solutions of the arc-shaped cavity flow with a variety of arc length ratio of $r=2/5, 1/3, 1/4, 1/5$ and $1/6$ are obtained. We find that for the arc-shaped cavity flow with arc length ratio less than $1/2$ ($r < 1/2$) there exist multiple steady solutions such that above a bifurcation Reynolds number two different solutions exist for a particular given Reynolds number. The wall-driven arcshaped cavity flow problem is not symmetric due to the geometry and also due to the boundary conditions and so is the two multiple solutions. We investigate the behaviour of the two different solutions as the Reynolds number changes and also as the arc length ratio of the arc-shaped cavity changes and we tabulate detailed results for future references. Our numerical solutions show that the bifurcation Reynolds number changes as the as the arc length ratio changes with the minimum bifurcation Reynolds number of 5164 at $1/3$ arc length ratio. We think that the arc-shaped cavity flow problem with arc

length ratio $r < 1/2$ is a unique flow problem for computational fluid dynamics field of study and further research on the arc-shaped cavity flow might reveal more solutions than the two solutions presented in this study.

REFERENCES

- Albensoeder, S., H. Kuhlmann and H. Rath (2001). Multiplicity of steady twodimensional flows in two-sided lid-driven cavities. *Theoretical and Computational Fluid Dynamics* 14(4), 223–241.
- Chen, K. T., C. C. Tsai, W. J. Luo and C. N. Chen (2013). Multiplicity of steady solutions in a two-sided lid-driven cavity with different aspect ratios. *Theoretical and Computational Fluid Dynamics* 27(6), 767–776.
- Ding, L., W. Shi, H. Luo and H. Zheng (2009). Investigation of incompressible flow within $1/2$ circular cavity using lattice boltzmann method. *International Journal for Numerical Methods in Fluids* 60(8), 919–936.
- Glowinski, R., G. Guidoboni and T. W. Pan (2006). Wall-driven incompressible viscous flow in a two-dimensional semicircular cavity. *Journal of Computational Physics* 216(1), 76–91.
- Lemée, T., G. Kasperski, G. Labrosse and R. Narayanan (2015). Multiple stable solutions in the 2d symmetrical two-sided square lid-driven cavity. *Computers & Fluids* 119, 204–212.
- Lomax, H. and J. Steger (1975). Relaxation methods in fluid mechanics. *Annual Review of Fluid Mechanics* 7(1), 63–88.
- Mercan, H. and K. Atalik (2009). Vortex formation in lid-driven arc-shape cavity flows at high reynolds numbers. *European Journal of Mechanics - B/Fluids* 28(1), 61–71.
- Migeon, C., A. Texier and G. Pineau (2000). Effects of lid-driven cavity shape on the flow establishment phase. *Journal of Fluids and Structures* 14(4), 469–488.
- Perumal, D. and A. Dass (2011). Multiplicity of steady solutions in two-dimensional lid-driven cavity flows by lattice boltzmann method. *Computers & Mathematics with Applications* 61(12), 3711–3721.
- Prasad, C. and A. Dass (2016). Use of an hoc scheme to determine the existence of multiple steady states in the antiparallel lid-driven flow in a two-sided square cavity. *Computers & Fluids* 140, 297–307.
- Shankar, P. and M. Deshpande (2000). Fluid mechanics in the driven cavity. *Annual Review of Fluid Mechanics* 32(1), 93–136.
- Wahba, E. (2009). Multiplicity of states for twosided and four-sided lid driven cavity flows. *Computers & Fluids* 38(2), 247–253.

E. Erturk / *JAFM*, Vol. 14, No. 4, pp. 1147-1163, 2021.

Yang, F., X. Shi, X. Guo and Q. Sai (2012). Mrt lattice boltzmann schemes for high reynolds number flow in two-dimensional lid-driven semi-circular cavity. *Energy Procedia* 16, 639–644.

Zhuo, C., C. Zhong, X. Guo and J. Cao (2015). Numerical investigation of four-lid-driven cavity flow bifurcation using the multiplerelaxation-time lattice boltzmann method. *Computers & Fluids* 110, 136–151.